Capillary phenomena in assemblies of parallel cylindrical fibers: From statics to dynamics

J.-B. Charpentier, Jorge César Brändle de Motta, T Ménard

Capillary phenomena in assemblies of parallel cylindrical fibers: from statics to dynamics

J.-B. Charpentier[a,b], J. C. Brändle de Motta[a,c,*], T. Ménard[a,c]

[a] *CNRS UMR 6614 CORIA, Saint-Étienne du Rouvray, France*
[b] *INSA de Rouen, Saint-Étienne du Rouvray, France*
[c] *Université de Rouen Normandie, Saint-Étienne du Rouvray, France*

Abstract

Among the tremendous amount of work that exists on spontaneous imbibition, the broadening of a fluid-fluid interface in a set of parallel fibers has not been tackled yet. Nevertheless, this problem is relevant to various applications. In a seminal paper, Princen derived a model which predicts the conditional existence of capillary bridges between pairs of fibers in remarkable lattices at the hydrostatic equilibrium. In the present work, it is argued that this model provides reliable predictions in dynamics. Therefore, the growth of these capillary bridges in a regular square lattice of parallel fibers has been studied through direct numerical simulations. In a dimensionless framework, the influence of the spacing of fibers, inertia, and viscosity and density ratios were investigated. The results show that Princen's predictions are in quantitative agreement with the observations. Furthermore, the temporal growths of capillary bridges are in qualitatively agreement with the Bosanquet's model. From the sensitivity study, it appears that the spacing parameters defines the pressure difference which drives the growth of capillary bridges. Inertia plays an insignificant role in the dynamics compared to the imbibition of a circular capillary. The non-wetting phase has a negligible influence on the flow in a liquid-gas system. Finally, a simulation in a complex disordered set of parallel fibers has been done. In such a system, the predictions of Princen's and Bosanquet's models are still

*Corresponding author
Email address: jorge.brandle@coria.fr (J. C. Brändle de Motta)

in qualitative agreement with the numerical simulations.

Keywords: Imbibition, Fiber medium, Two-Phase flow, CLSVoF

1. Introduction

Wetting of a fiber medium is ubiquitous in both nature and industry. In nature, fur of animals is a means to resist the infiltration of water to the skin and to speed up the drying after water exposure (Dickerson et al., 2012). In the industry, fiber yarns are used to make clothes, the ability of water to wet the fibers of these yarns influences water exchanges between the body and the atmosphere and therefore changes the comfort felt (Patnaik et al., 2006). In particular, the local relative orientation of fibers within yarns influences the efficiency of drying (Boulogne et al., 2015). In certain composite material processes, rigid fibers are mixed with a liquid resin. Depending on the wetting properties of fibers, the outcome of this process may be a stiff light material or a fragile unusable one (Pucci et al., 2017; Testoni et al., 2018). Fiber wetting can also be tuned in order to build complex organized self-assembled structures which may capture particles or produce a particular surface texture (Pokroy et al., 2009; Chandra and Yang, 2009). Many other examples may be found (see e.g. Duprat et al. (2012); Wang et al. (2017)) and several aspects of fiber media wetting are still ongoing research topics. Fibrous media have two specific features when exposed to fluid-fluid interfaces. First, fibers flexibility makes them sensitive to the action of capillary forces which may induce strains, bond the fibers and assemble them into clusters (Bico et al., 2004). Second, even in the case of an undeformable, simple and regular arrangement of fibers, the static equilibrium of two fluids within this arrangement can be complex. These features are of importance in the applications mentioned above, and they are both related to the existence of a broad fluid-fluid interface characteristic of open capillaries. Princen derived a model which shows that pressure differences and thus capillary bridges may exist between pairs of fibers when a periodic lattice of parallel fibers is dipped into a liquid bath (Princen, 1969a,b). This model has been ap-

plied or generalized in various situations and seems quite robust, even when the slenderness of the system, required in the derivation, is questionable (Protiere et al., 2013; Soleimani et al., 2015; Boulogne et al., 2015; Sauret et al., 2015). To our knowledge, in dynamics, neither the applicability of Princen's model nor the growth of capillary bridges in a remarkable or complex fibrous network has been studied yet. This growth is a spontaneous imbibition in the sense that it consists of a flow from the bottom of a capillary bridge to its top and is driven by capillary forces. The spontaneous imbibition of simple systems or media have been intensively studied in the past decades. A detailed understanding of its physics has been established. The most considered configuration is a circular cross section tube of small radius dipped into a wetting liquid bath. In this case a liquid column rises into the tube under the action of capillary forces. In the very first instants a meniscus forms and creates a pressure difference between the meniscus and the liquid bath. This pressure difference drives the flow and depends on surface tension and of the meniscus curvature which is itself a function of the tube radius and of the viscous dissipation at the triple line. At this point, inertia and/or viscous dissipation balances the driving pressure difference. After some time, a static equilibrium is reached at Jurin's height, when the columns weight balances capillary forces. The equation of Washburn (see Washburn (1921) and also Bosanquet (1923)), which describe the temporal evolution of the meniscus position within the tube, predicts the existence of a few regimes. In a given problem, the relevant regimes depend on the ratios of viscous dissipation, inertia and gravity to capillarity. For example, when the bulk viscous dissipation balances capillarity, the meniscus position X scales as $X \propto t^{1/2}$ and when inertia balances capillarity it scales as $X \propto t$. In the literature, the observations are in an overall good agreement with the various model predictions (Quéré, 1997; Chebbi, 2007; Reyssat et al., 2008; Fries and Dreyer, 2008; Digilov, 2008; Figliuzzi and Buie, 2013). Although often neglected, depending on its viscosity and density the surrounding non-wetting fluid may play a significant role on the imbitition dynamics (Hultmark et al., 2011; Walls et al., 2016). The imbibition of open capillaries (grooves, wedges) is slightly different.

For a wedge, there is a critical opening angle condition which defines if the imbibition is possible (Concus and Finn, 1969). Owing to the indefinitely small characteristic length in the wedge, there is no Jurin's height, the capillary rise is theoretically unbounded and asymptotically the wetting fluid front scale as $X \propto t^{1/3}$ (Tang and Tang, 1994; Ponomarenko et al., 2011). In the case of a set of parallel fibers, the growth of capillary bridges is a specific case of a spontaneous imbibition in a set of open capillaries. However, in this situation the pressure difference is bounded as long as the spacing between the fibers is not null. In porous media, imbibition and drainage lead to the broadening of the fluid-fluid interface. Depending on the mechanisms at play, different temporal evolution of the interface width with time were predicted and reported (Wilkinson, 1984; Horváth and Stanley, 1995; Dubé et al., 2007; Sadjadi and Rieger, 2013). To our knowledge, highly anisotropic fiber media such as yarns have not been considered yet. Therefore, there is no observation nor prediction in this particular case. Experimentally, tracking and recording a fluid-fluid interface in a yarn is difficult to perform. As a consequence, in this work, the growth of capillary bridges in an infinite square lattice of parallel fibers is simulated. The aim of the present paper is to:

- Question the robustness of Princen's model in dynamics, i.e., compare the pressures predicted by the model (static) to the pressures computed in the simulations (dynamic).
- Understand the growth of capillary bridges and its sensitivity to the main parameters of this problem, i.e., observe the temporal evolution of the length of capillary bridges and relate this observation to the spacing between the fibers, inertia and the viscosity and density of the non-wetting fluid.
- Question its own relevance to describe the broadening of the fluid-fluid interface in yarns, i.e., compare the reported pressures and growths obtained in ordered and disordered lattices.

Recently, new numerical methods have been developed to treat the fluid-fluid interface and to account for contact angles. These technics provide new ways to investigate wetting related applications with static or dynamic contact angles. For example, the spreading of a droplet on a porous medium has been simulated (Aboukhedr et al., 2018) or through a randomly generated porous medium (Sadeghi et al., 2018), two-phase flows at microfluidics junctions (Chen et al., 2012), or the detachment of a droplet from a horizontal fiber (Wang and Desjardins, 2018a,b) with a static contact angle. In these applications, the numerical predictions were found to provide reliable descriptions when compared to experimental data. However, in problems involving rapid motions of the triple line the dissipation in its vicinity plays a key role. Thus, different authors developed numerical strategies to implement dynamic contact angle models (Yokoi et al., 2009; Malgarinos et al., 2014; Akai et al., 2018). In applications such as the imbibition of a capillary and the impact of a drop on a surface, these strategies improved substantially the match between numerical simulation and experiments. In particular, some of these methods are able to handle complex geometries into Cartesian grids (Arienti and Sussman, 2014; Lepilliez et al., 2016; Wang and Desjardins, 2018a). In this work, the in-house ARCHER code has been extended to model static contact angles with these methods and used to model the growth of capillary bridges in an assembly of parallel cylindrical fibers.

This manuscript is organized in the following way. In section 2, the governing equations and the numerical methods are briefly presented in a dimensionless framework. The implementation in the in-house code ARCHER is validated through two canonical problems where wetting plays a key role. In section 3, Princen's derivation in the case of a regular square lattice of parallel fiber is presented. Then, it is argued that the predictions of the model should still be of relevance in dynamics. In section 4, the regular lattice simulations results are presented and discussed varying the independent dimensionless parameters and compared to the predictions. In section 5, the results obtained with a disordered set of parallel fibers are discussed and compared to Princen's predictions. Fi-

nally, the main conclusions and implications of this work are reported in section 6.

2. Numerical approach and validation

2.1. Governing equations

In this work, two fluids and a non-deformable fixed solid are considered in a 3D domain. The fluids are partially wetting and partially non-wetting and are here referred as the wetting and the non-wetting fluid respectively. The contact angle θ_e is assumed to be small over the entire study such that the hysteresis effects are expected to be small as well. In the following sections, the wetting fluid will be denser than the non-wetting one. Both fluids are assumed to be initially static, therefore capillarity drives the flow. Since the velocities involved in such problems are relatively small compared to the speed of sound in both fluids, the flow is assumed to be incompressible. Thus, the densities of both fluids ρ_α are considered as constant. Here α subscript designates the wetting fluid w or the non-wetting one nw. Both are considered as Newtonian with a viscosity μ_α. Finally, the surface tension γ, is kept constant since no temperature or chemical potential evolution is considered. In order to reduce the number of truly independent parameters, the incompressible Navier-Stokes equations are turned dimensionless. A characteristic length R, which depends on the system, is used to set all distances into a dimensionless form. In the upcoming sections, R is a drop, a capillary or a fiber radius. The pressure P is turned dimensionless with the capillary pressure γ/R, $\widetilde{P} = PR/\gamma$. Finally, the time t, is divided by the capillary time of the wetting fluid, $t_\mu = \mu_w R/\gamma$, such that $\tilde{t} = t/t_\mu$. Using the above mentioned dimensionless variables, the incompressible Navier-Stokes equations write:

$$\nabla \cdot \widetilde{\vec{v}}_\alpha = 0 \tag{1}$$

$$La\left(\frac{\partial \widetilde{\vec{v}}_w}{\partial \widetilde{t}} + (\widetilde{\vec{v}}_w \cdot \vec{\nabla})\widetilde{\vec{v}}_w\right) = \nabla \cdot \widetilde{\vec{D}}_w - \vec{\nabla}\widetilde{P}_w + Bo\vec{e}_g \tag{2}$$

$$LaM_\rho\left(\frac{\partial \widetilde{\vec{v}}_{nw}}{\partial \widetilde{t}} + (\widetilde{\vec{v}}_{nw} \cdot \vec{\nabla})\widetilde{\vec{v}}_{nw}\right) = M_\mu \nabla \cdot \widetilde{\vec{D}}_{nw} - \vec{\nabla}\widetilde{P}_{nw} + M_\rho Bo\vec{e}_g \tag{3}$$

where equation 1 is solved on both fluid domains, the equation 2 on the wetting fluid domain and the equation 3 on the non-wetting one. ∇ is the gradient operator and $\widetilde{\vec{D}}_\alpha$ is the dimensionless stress tensor, $\widetilde{\vec{D}}_\alpha = \frac{1}{2}\left(\nabla\widetilde{\vec{v}}_\alpha + (\nabla\widetilde{\vec{v}}_\alpha)^t\right)$. La is the Laplace number, $La = \rho_w\gamma R/\mu_w^2$, that is a balance of inertia, viscosity and capillarity. Bo is the Bond number, $Bo = \rho_w g R^2/\gamma$, that is the balance of gravity to capillarity and $\vec{e}_g$ is the unit vector of the gravity field. $M_\rho = \rho_{nw}/\rho_w$ and $M_\mu = \mu_{nw}/\mu_w$ are the density and viscosity ratio respectively. Note that the inertial time of the wetting fluid $t_\rho = \sqrt{\rho_w R^3/\gamma}$ which is relevant for inertia and capillary phenomena writes $\widetilde{t}_\rho = t_\rho/t_\mu = La^{1/2}$. The continuity of velocities across the interface is also assumed since no phase change is considered. With the above-stated set of dimensionless equations, the normal force balance at the surface given by the Young-Laplace equation reduces to

$$\vec{n} \cdot \left(\left(\widetilde{P}_{nw} - \widetilde{P}_w\right)\mathbf{I} - 2\left(M_\mu\widetilde{\vec{D}}_{nw} - \widetilde{\vec{D}}_w\right)\right) \cdot \vec{n} = \widetilde{\kappa}, \tag{4}$$

where $\mathbf{I}$ is the identity tensor and $\widetilde{\kappa} = \kappa R$ is the dimensionless curvature and $\vec{n}$ the normal to the interface. The tangential stress balance is written using the unitary vector tangential to the interface $\vec{t}$,

$$\vec{t} \cdot \left(M_\mu\widetilde{\vec{D}}_{nw} - \widetilde{\vec{D}}_w\right) \cdot \vec{n} = 0. \tag{5}$$

Velocities are null at both fluid-solid boundaries. Finally, the fluid-fluid interface meets the solid with an angle θ_e, as described by the Young-Dupré equation. To solve this general set of equations, a robust and accurate method

is needed. The following section details the numerical approach used in this work.

2.2. Numerical method

The present numerical study has been performed with the in-house two-phase flow Navier-Stokes solver ARCHER. It was initially developed to treat incompressible liquid-gas flows (Ménard et al., 2007), in particular, this code has been used intensively to analyze spray atomization (see e.g. Vaudor et al. (2017); Asuri Mukundan et al. (2019)). In order to reproduce this kind of harsh applications, a method able to provide an accurate description of the interface and which respects mass and momentum conservation must be used (Vaudor et al., 2017). These features, which are also suitable in the present work, derive from the following set of choices. First, the two-phase incompressible Navier-Stokes equations are solved on a staggered Cartesian mesh using a projection method increasing both the accuracy and the stability of the solution. The Poisson equation is solved using a conjugate gradient method and takes into account the pressure and density jump across the interface. The convective term of Navier-Stokes equations is computed through a 5th order method in order to capture the sharp interface while the viscous terms are computed with the discretization proposed by Sussman et al. (2007). The flux computation for mass and momentum are consistent in order to increase the robustness of the method (Vaudor et al., 2017). Second, the two-phase flow description is based on the coupled Level-Set Volume of Fluid (CLSVoF) method (Ménard et al., 2007). In this framework, the fluid-fluid interface is described through a signed distance function ϕ and the local denser fluid volume C. Both are defined at each cell center. The Level-Set function allows the computation of the normal to the interface $\mathbf{n} = \frac{\nabla\phi}{|\nabla\phi|}$ which itself allows the computation of the curvature $\kappa = -\nabla \cdot \mathbf{n}$. By coupling the Level-Set and the VoF our code remains second order on the computation of curvatures and respects the mass conservation. In order to maintain the accuracy of the computation, the Level-Set has to remain a distance function, $|\nabla\phi| = 1$. This condition is guaranteed through a

re-initialization procedure performed at each time step. This procedure consists in solving the equation:

$$\frac{\partial \phi}{\partial \tau} + \text{sign}(\phi_0)\left(|\nabla \phi| - 1\right) = 0 \tag{6}$$

where, τ is a fictitious time and ϕ_0 is the Level-Set function before the re-initialization procedure. Typically, only a few iterations are needed to reach a stationary solution. In the present simulations, since the interface evolution is slow, two iterations of re-initialization are done after each time step. After these two iterations, the resulting Level-Set is then used for the next time step. Third, in order to take into account the presence of one or multiple solids of arbitrary shapes in the Cartesian domain, an immersed boundary method is used (Vu, 2017). The selected method considers a sharp interface between the solid and the fluids domains through a signed distance function ϕ_s. One of the main advantages of this method, originally developed by Ng et al. (2009) for single-phase flows, is that it respects the symmetry of the Poisson solver matrix. An extension of this method to two-phase flow was proposed recently by Lepilliez et al. (2016) providing an accurate treatment of the contact line. Therefore, this improved method is used in this work to describe the flow around the immersed solid. In order to respect the Young-Dupré equation, the contact angle must be imposed at each time step where the fluid-fluid interface meets the solid. This is imposed through a contact angle procedure which solves the following equation into the solid region:

$$\frac{\partial \phi}{\partial \tau} + \nabla \phi \cdot \nabla \phi_s = \cos(\theta_e) \tag{7}$$

where, τ is a fictitious time. The figure 1 provides an illustration of the effect of the contact angle procedure. In the present method, the equilibrium contact angle θ_e is fixed. As explained in section 2.3 and 2.4, a fixed contact angle does take into account a part of the viscous dissipation near the triple line without the use of an analytical or empirical model. Finally, the use of a Level-Set to describe the fluid-fluid interface in the vicinity of a curved solid can cause

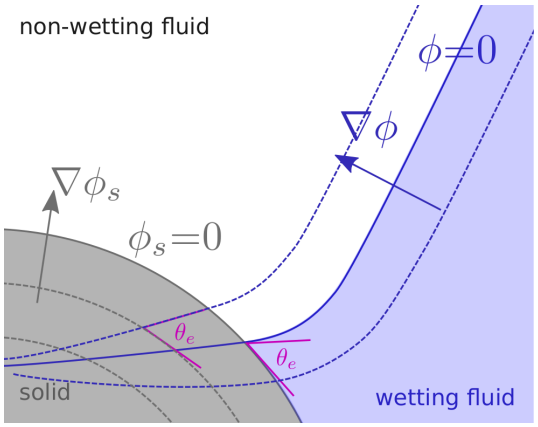

Figure 1: Sketch of the description of the contact line in the numerical method. The discontinuous curves in blue and grey represent isovalue lines of the non-wetting fluid and solid Level-Sets respectively

numerical difficulties as the contact angle tends to be 0 or π (Xu and Ren, 2016). However, with a Cartesian grid with a fixed grid spacing, when the contact angle tends to these limits the description of the flow is insufficient in the confined fluid domain (in the wedge near the triple line). Therefore, in the targeted applications such a correction does not change the range of angles that can be used. In the following sections, the angle will be set at $\theta_e = 10°$ unless stated otherwise and the curvature of the solids will always be clearly greater than the grid spacing.

Since the accuracy of the fluid-fluid interface treatment has already been proven in the past, only validations of the triple line treatment are here addressed.

2.3. Drop spreading on a flat surface

In order to show the ability of the previously described numerical method to model a two-phase flow with a solid, simulations of the spreading of a liquid drop on a flat substrate are carried out. The spreading of a partially wetting drop is a canonical problem that has been studied through experimental, analytical and numerical methods (Biance et al., 2004; Bird et al., 2008; Winkels et al., 2012; Wang and Desjardins, 2018a; Legendre and Maglio, 2013). In this problem a

drop of initial radius R comes in contact with a solid substrate with a vanishingly small velocity and then spreads on it such that the drop radius on the substrates r increases with time. In the early instants of the spreading, inertia balances capillarity and a first regime is encountered with $\widetilde{r} \propto t^{1/2}$ (Biance et al., 2004; Bird et al., 2008; Winkels et al., 2012) with $\widetilde{r} = r/R$. As the drop tends to take the shape of a spherical cap, viscosity comes into play and controls the flow near the triple line. In later stages, this viscous dissipation controls the evolution of the drop radius with time such that $\widetilde{r} \propto \widetilde{t}^{1/10}$. This second relation is generally referred to as Tanner's law (Tanner, 1979). The evolution of the drop radius is bounded for finite contact angles and mass conservation gives: $\widetilde{r}_{max} = \left(4\sin^3(\theta_e)/(2-\cos(\theta_e))(3-\cos^2(\theta_e))\right)^{1/3}$ for a dimensionless initial drop radius of 1. The transition time from the inertial to the viscous regime is a function of drop radius, surface tension, fluid density, and viscosity. In a dimensionless form it is expected to be proportional to $La^{5/8}$ (Biance et al., 2004). However, for viscous fluids, the inertial regime is not observed and a new relation of the form $\widetilde{r} \propto \widetilde{t}^{2/3}$ appears. In the present numerical model, a spherical drop of radius $\widetilde{R} = 1$ is initially put in contact with a solid substrate defined throughout the solid Level-Set. The initial radius on the substrate is $\widetilde{r}(\widetilde{t} = 0) = 0.3$. The second fluid is assumed to have a negligible influence on the flow therefore the density and viscosity ratios are equal and $M_\mu = M_\rho = 10^{-3}$. The contact angle is $\theta_e = 10°$, which gives $r_{max} = 3.1$. The Laplace number is varied from 1 to 10^3 on 7 values evenly spaced on a log scale. Using the axisymmetry of the problem, only a quarter of the domain is simulated. Symmetry boundary conditions are applied to both boundaries near the drop center and a fixed pressure boundary condition is applied to other ones. Thus, the domain is a square with ridges of length 2.7 and the grid spacing is 0.35. The initial and boundary conditions are represented on figure 2a.

Images of a simulated drop spreading are presented on figure 2b. The evolution of drop radius $\widetilde{r}$ with time $\widetilde{t}$ is represented on figure 2c. On the figure, for all values of La the radius reaches quickly a first regime where $\widetilde{r} \propto \widetilde{t}^n$. The value of n is about 0.5 for large La and is larger for lower values of La. The

curves obtained for large La values tends to collapse when represented as a function of the dimensionless inertial time $\widetilde{t}/La^{1/2}$ as it may be seen on figure 2d. Therefore, this first regime corresponds to the above described inertial regime. Then, a change of slope appears in the log-log plot at similar values of $\widetilde{t}$ for all La. This implies the existence of a relation of the form $\widetilde{r} \propto \widetilde{t}^m$ with $m \sim 0.11$. In this regime, all curves tend to collapse when represented as a function of $\widetilde{t}$. Therefore, this second regime matches the features of the viscous one. Finally, a simulation result of Wang and Desjardins (2018a) done with a contact angle of 10°, a Laplace number $La = 10.3$, a density ratio of $M_\rho = 1.03 \times 10^{-3}$ and a viscosity ratio of $M_\mu = 2.89 \times 10^{-4}$ is plotted on figures 2c and 2d. The parameters used in this simulation are similar to the one of the presently reported results with $La = 10$. On both figures, it appears that their result is in very good agreement with ours in the inertial regime. In the viscous regime, the evolution of r with time takes also the form $\widetilde{r} \propto \widetilde{t}^m$ but with a coefficient $m \sim 0.085$. These different slopes are both close to the theoretical prediction. Nevertheless, this later regime is very sensitive to the dissipation at the triple line. The difference observed are attributed to the different methods used to describe the triple line.

The observation of both regimes shows the ability of the method to simulate a capillary driven phenomenon balanced by inertia and/or viscosity in a wide range of La. More specifically, the viscous regime shows that the dissipation is properly described near the triple line down to the grid spacing scale and that this description is sufficient to catch the main features of the above treated example. The same observation may be applied to other published works with a comparable accuracy (Wang and Desjardins, 2018a).

2.4. Spontaneous imbibition of a circular capillary

The previously described drop spreading problem involved a flat substrate, in order to validate the method with a curved geometry, the imbibition of a circular capillary is simulated. As described in the introduction, this problem has been widely investigated and its physics is well understood. In particular, when a

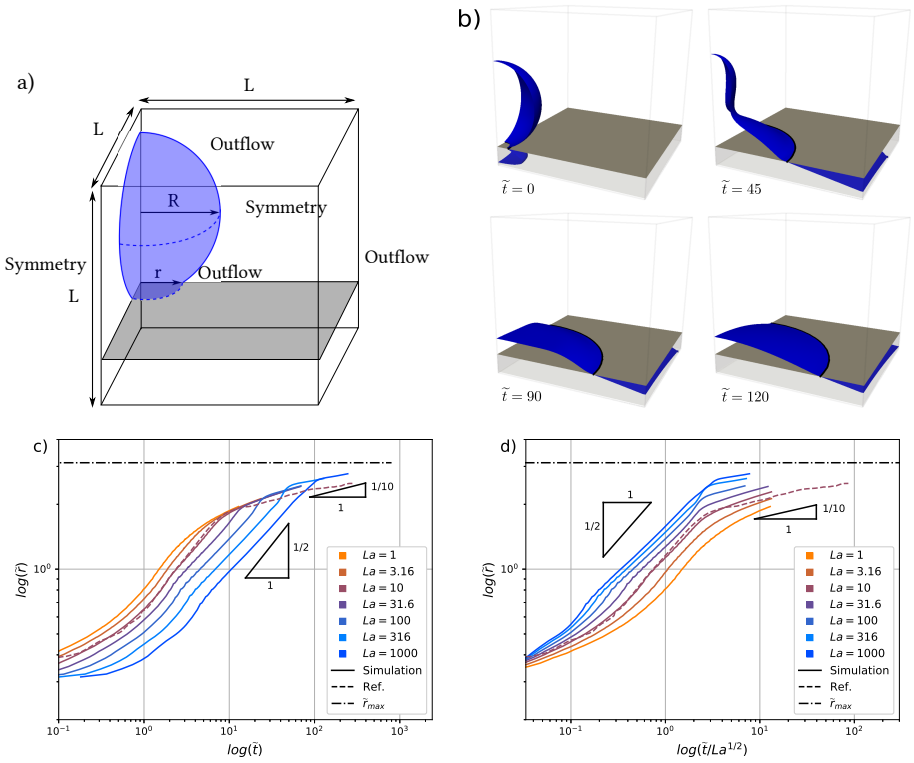

Figure 2: (a) Sketch of the drop spreading simulation at $\widetilde{t} = 0$. (b) Images of a drop spreading with $La = 1000$ at different instants. See the Electronic Annex in the online version of this article for the corresponding video. Dimensionless spreading radius $\widetilde{r}$ as a function of: (c) the dimensionless time $\widetilde{t}$ and (d) the inertial dimensionless time $\widetilde{t}/La^{1/2}$. In the legend, Ref. refers to Wang and Desjardins (2018a).

wetting, dense and viscous fluid invades a circular capillary initially filled with a low density, low viscosity fluid and without gravity, the model of Bosanquet (Bosanquet, 1923) describes the evolution of the meniscus position with time. Noting X the meniscus position measured from the capillary entrance and taking R, the capillary radius, as the characteristic length, Bosanquet's equation takes the dimensionless form:

$$La\frac{d}{d\widetilde{t}}\left(\widetilde{X}\frac{d\widetilde{X}}{d\widetilde{t}}\right) = 2\cos\left(\theta_d\right) - 8\left(\widetilde{X}\frac{d\widetilde{X}}{d\widetilde{t}}\right) \tag{8}$$

where θ_d is the dynamic contact angle. For small values of equilibrium contact angle θ_e, an important viscous dissipation is expected at the triple line such that $\theta_d > \theta_e$. Physically, a gradient of curvature is expected such that the contact angle at the microscopic level is indeed the equilibrium contact angle θ_e and such that the macroscale (or apparent) contact angle is θ_d. For small contact angles, the dissipation can be computed with the model of de Gennes (de Gennes, 1985), which reads:

$$\tan\left(\theta_d\right)\left(\theta_e^2 - \theta_d^2\right) = 6\Gamma\dot{\widetilde{X}}. \tag{9}$$

In this equation $\Gamma = \log(l_1/l_2)$ where l_1 and l_2 are the macro and micro scale characteristic lengths respectively. In the numerical simulations, the contact angle is set at its equilibrium value at the grid spacing scale. Therefore, the viscous dissipation near the triple line exists and the Γ parameter should be $\Gamma = \log\left(1/\Delta\widetilde{X}\right)$, with $\Delta\widetilde{X}$ the grid spacing. It is worth noticing that this value of Γ is smaller than the corresponding value in the real physical problem where the micro scale characteristic lengths is related to the size of the fluid molecules. All simulations were done with a capillary of radius $\widetilde{R} = 1$ in a rectangular simulation box of dimensions, $\widetilde{l} = 1.05$ and $\widetilde{L} = 16.8$ (see figure 3a). Using symmetry boundary conditions, a quarter of the domain is simulated. The mesh grid is fixed to $16 \times 16 \times 256$. Both extremities of the capillary are set to the same fixed pressure, $\widetilde{P} = 0$. Initially, the capillary is filled with the wetting fluid along a distance $\widetilde{X}_0 = 0.05$. The second fluid density and viscosity

are set to low values, $M_\mu = M_\rho = 10^{-3}$. The Laplace number is set to 50 and the contact angle is varied within the set of values 10, 20, 40 and 60. Images of the imbibition are presented on figure 3b at various instants. The evolution of the bottom position of the meniscus $\widetilde{X}$ with time $\widetilde{t}$ is reported on figure 3c with the prediction of Bosanquet's model (equation 8) without a dynamic contact angle. Figure 3c shows that this model overestimates widely the imbibition dynamics. Predictions with a dynamic contact angle and a parameter $\Gamma = 2.7$ (computed with the above mentioned method) are also reported on the figure. Taking into account the viscous dissipation near the triple line improves the matching. The results reported for $\theta_e = 20,\ 40°$ are in excellent agreement with the dynamic angle model. However, the application of de Gennes' model for angles as high as 40° and 60° is questionable. On the other hand, with a small contact angle ($\theta_e = 10°$) the wetting fluid Navier-Stokes equations are solved in a very confined volume near the triple line. Therefore, the description of the flow in this volume is rough due to an insufficient mesh resolution. The approximate matching reported on figure 3c with $\theta_e = 10°$ has been attributed to this rough description of the viscous dissipation at the triple line. Nevertheless, the main features of the imbibition dynamics are still well reproduced and the temporal evolution of the meniscus position is in a rough quantitative agreement with the model.

The temporal evolution of the meniscus position with time in the spontaneous imbibition simulations of a circular capillary are in an overall good agreement with Bosanquet's predictions when a dynamic contact angle model is used. These results show that the contact angle is properly imposed at the triple line with a curved immersed boundary. Furthermore, the viscous dissipation at the triple line is taken into account (within the range of scale simulated) and is in qualitative agreement with de Gennes' model.

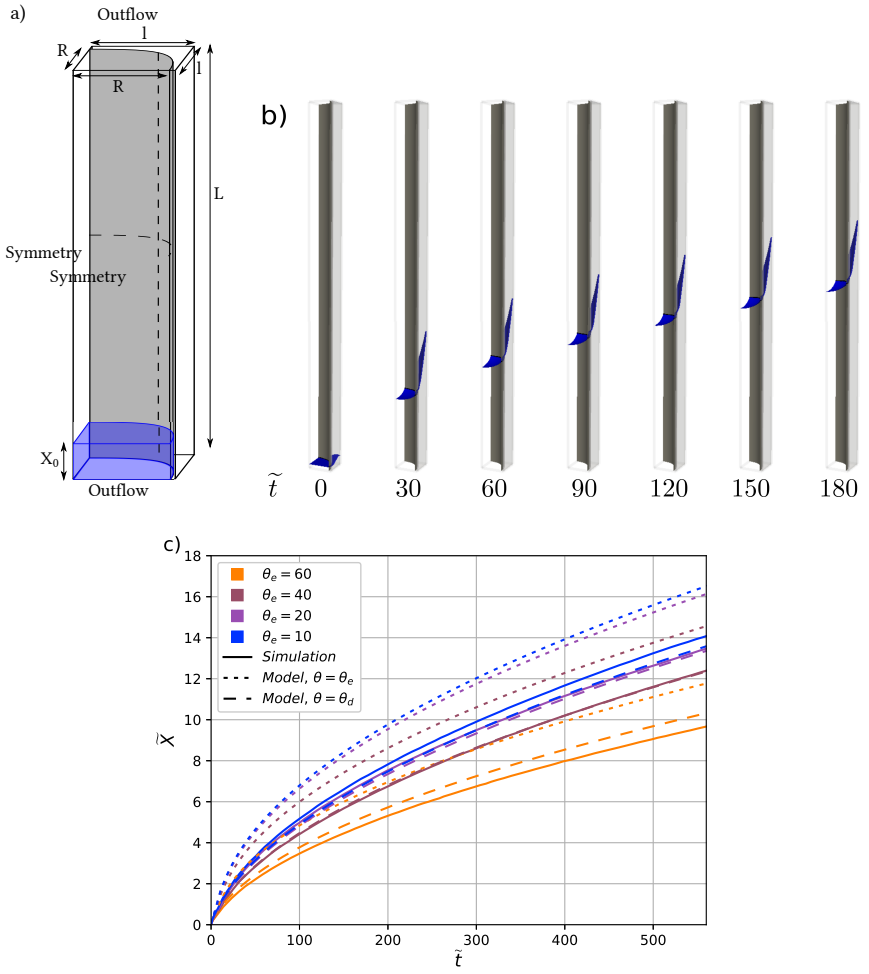

Figure 3: (a) Sketch of the capillary imbibition simulation at $\widetilde{t} = 0$. (b) Images of the imbibition at various instants with $\theta_e = 10^{circ}$. See the Electronic Annex in the online version of this article for the corresponding video. (c) Position of the meniscus $\widetilde{X}$ as a function of time $\widetilde{t}$. In the legend, "model $\theta = \theta_e$" refers to the solution of equation (8) for a fixed contact angle and "model $\theta = \theta_d$" to the solution of equation (8) with a dynamic contact angle described by equation (9)

3. Static equilibrium and imbibition dynamics in a periodic lattice of fibers

3.1. Static equilibrium in a periodic lattice

In his seminal work, Princen (Princen, 1969a,b) considered various systems corresponding to different spatial organization of parallel fibers. In one of them, the fibers formed a regular square lattice of parallel fibers with a constant spacing $2d$. In his derivation, the system used was a unit cell of the lattice such as represented on figure 4. Princen considered the static equilibrium reached by a dense wetting fluid in the void when capillarity is balanced by gravity. Two cases were distinguished. In the first one, I, the capillary rise reaches a unique height h_I at which the fluid-void interface is formed. Under this height the medium is saturated with the dense wetting fluid (see figure 4). In the second one, II, above the previously described equilibrium, liquid bridges exist between pairs of fibers. Therefore a first fluid-void interface exists at a height $h_{II,b}$ and extends toward the tip of capillary bridges at a height $h_{II,a}$ (see figure 4). The transition from I to II depends on the spacing between fibers. As the hydrostatic equilibrium is assumed, each height corresponds to a unique pressure. For a slender system, such that the height of rise is widely greater than the fiber radius R, the capillary pressure can be computed directly from the surface tension and the in-plane curvature R^* (see figure 4). Furthermore, both extremities of capillary bridges have negligible depths. Therefore, the pressure at the meniscus (or at the end of a capillary bridge) can be computed assuming the equilibrium of a small system along the fiber axis. In the single height case I, the equilibrium gives:

$$\widetilde{P}_I = -\frac{2\pi\cos(\theta_e)}{4(1+\widetilde{d})^2-\pi}. \tag{10}$$

In the second one, following the same arguments, the meniscus pressure is computed as

$$\widetilde{P}_{II,b} = -\frac{(2\pi-8\alpha)\cos(\theta_e)+8\beta\widetilde{R}^*}{4(1+\widetilde{d})^2-\pi-4\widetilde{A}}, \tag{11}$$

and the pressure at the tip of capillary bridges as

$$\widetilde{P}_{II,a} = -\frac{8\alpha\cos(\theta_e) - 8\beta\widetilde{R}^*}{4\widetilde{A}}. \tag{12}$$

In the above equations, β is geometrically related to α and θ_e:

$$\alpha + \beta + \theta_e = \frac{\pi}{2}, \tag{13}$$

the radius $\widetilde{R}^*$ is expressed as

$$\widetilde{R}^* = \frac{1 + \widetilde{d} - \cos(\alpha)}{\sin(\beta)}, \tag{14}$$

and $\widetilde{A}$ is half the area of wetting fluid between two fibers:

$$\widetilde{A} = 2\widetilde{R}^*\sin(\alpha)\sin(\beta) - (\alpha - \sin(\alpha)\cos(\alpha)) - \widetilde{R}^{*2}(\beta - \sin(\beta)\cos(\beta)). \tag{15}$$

In case II, α, β, $\widetilde{R}^*$ and $\widetilde{A}$ vary continuously from the tip (a) to the bottom (b) of capillary bridges.

The key assumptions of this derivation are, that (i) the system length is widely greater than the radius of the fibers (ii) interfaces are shaped by capillarity ($Bo \ll 1$) (iii) the contact angle is constant. In the literature, the sensitivity to the slenderness of the system has not been studied. However various authors reported results in agreement with Princen's predictions for two fibers with rather low slenderness (Boulogne et al., 2015; Sauret et al., 2015; Soleimani et al., 2015).

3.2. Dynamics in a periodic lattice

In dynamics and without gravity ($Bo = 0$), capillarity rules the shape of the fluid-fluid interface as long as inertia and viscosity are both small ahead of capillary forces, which writes: $\rho v^2 R/\gamma = We \ll 1$ and $v\mu/\gamma = Ca \ll 1$. Furthermore, the contact angle is expected to be constant and equal to θ_e for small values of Ca. Therefore, if a capillary bridge is slender enough and its growth is slow enough then Princen's model requirements are met in

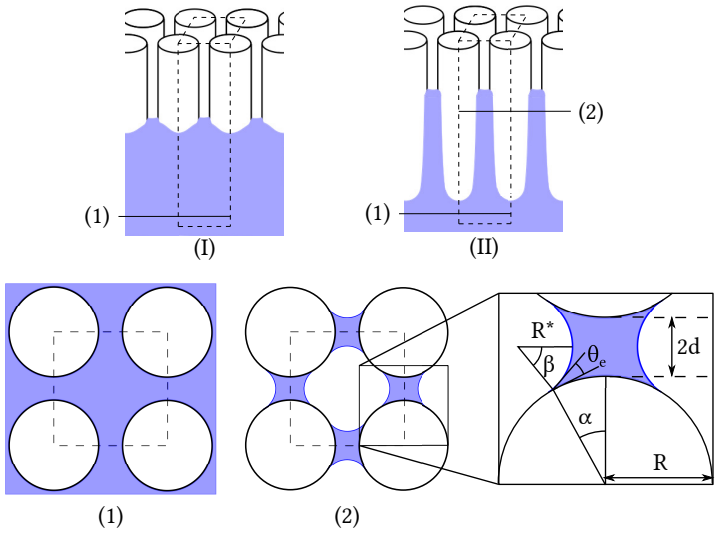

Figure 4: Sketch of Princen's system in the case of a square lattice of parallel fibers with a spacing parameter d. On the figure, (I) and (II) refer to the cases without and with capillary bridges respectively. (1) and (2) refer to slices of the system considered at different heights.

dynamics. Thus, the predictions of his model, i.e., the pressures $\widetilde{P}_I$, $\widetilde{P}_{II,a}$ and $\widetilde{P}_{II,b}$, should be encountered in dynamics. In case II, the pressure difference $\Delta\widetilde{P} = \widetilde{P}_{II,b} - \widetilde{P}_{II,a}$ should drive the formation of capillary bridges between pairs of fibers. Remarking that for a given spacing parameter $\widetilde{d}$, the area A filled by the wetting fluid exhibits small variations between the tip and the bottom of capillary bridges. Therefore, the growth of capillary bridges can be roughly described as the imbibition of a closed capillary through Bosanquet's equation. In our dimensionless framework, this equation writes:

$$La\frac{d}{d\widetilde{t}}\left(\widetilde{X}\frac{d\widetilde{X}}{d\widetilde{t}}\right) = -\Delta\widetilde{P} - \frac{1}{\widetilde{K}}\left(\widetilde{X}\frac{d\widetilde{X}}{d\widetilde{t}}\right), \tag{16}$$

where $\widetilde{K}$ represents the permeability of the wetting fluid between the fibers and may be roughly estimated by equation A.6 (see appendix Appendix A). According to its derivation, $\widetilde{K}$ is a function of α which varies monotonically from the tip to the bottom of capillary bridges. As a consequence, the extreme values of $\widetilde{K}$ provide bounds within which the effective value should stand. Although

this model has some strong limitations (it neglects the second fluid, the real geometric complexity of the problem, *etc.*), it provides a simple description of the growth of capillary bridges.

4. Growth of capillary bridges in a periodic lattice of fibers

4.1. Simulation set-up

The growth of capillary bridges in a unit cell of a regular square lattice of parallel fibers is simulated. Using the system's symmetries, symmetric boundary conditions are applied to four sides and only a quarter of the unit cell is modeled thus reducing the volume of the computational domain. The fluid velocity is set to zero at the lower boundary and the pressure is set to zero at the upper one. In the unit cell, the fiber is modeled as a perfect cylinder of radius $\widetilde{R} = 1$ represented by the solid Level-Set. The domain have a rectangular section of ridge $\widetilde{l} = 1 + \widetilde{d}$ and a height of $\widetilde{L} = 9\,\widetilde{l}$. At the beginning of each simulation, the domain is filled with the dense wetting fluid over a length $\widetilde{X}_0 = 2\widetilde{l}$. A sketch of the simulated problem at $\widetilde{t} = 0$ is presented on figure 5a. After a convergence study, the domain has been decomposed into $32 \times 32 \times 288$ mesh nodes (see Electronic Annex in the online version of this article for more details.).

The computational cost is directly related to the number of the time steps, the number of cells, the number of processors, and the time step that is limited by the velocity of capillary waves . Hence, the Laplace number has a great impact on the computational cost. The computations were performed in different clusters with different specifications. The reference simulation was simulated for 115 hours using 9 cpu cores (Intel Xeon 8168 (SKL), 2.7 GHz). This simulation iterates over 3.5×10^5 time steps to reach the end of the simulation at $\widetilde{t} = 1.1 \times 10^3$.

The impact of the parameters: $\widetilde{d}$, La, M_μ and M_ρ are investigated for a given value of $\theta_e = 10°$. Compared to a reference case each parameter is varied for the same fixed values of the three others. The reference case parameters are $La = 1000$, $M_\mu = 10^{-3}$, $M_\rho = 10^{-3}$ and $\widetilde{d} = 0.1$. Images of the corresponding

simulation are presented on figure 5c. $\widetilde{d}$ is varied from 0.075 to 0.2, La from 1 to 10^5. Finally, M_μ and M_ρ are varied from 10^{-3} to 3.16×10^{-2}. Results are presented in the same order in the following sections.

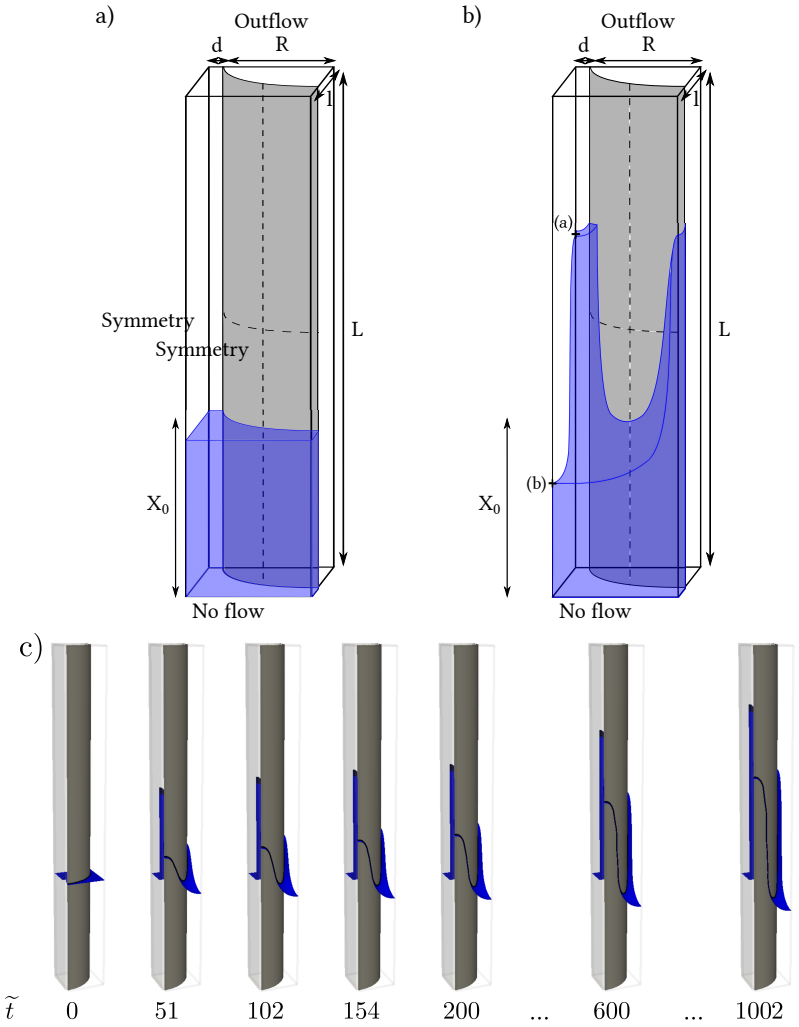

Figure 5: (a) Sketch of the imbibition at $\widetilde{t} = 0$ and (b) at $\widetilde{t} > 0$. (c) Images of the imbibition in the reference case ($La = 1000$, $M_\mu = 10^{-3}$, $M_\rho = 10^{-3}$, $\widetilde{d} = 0.1$) at various instants. See the Electronic Annex in the online version of this article for the corresponding video.

4.2. Influence of $\widetilde{d}$

The spacing parameter $\widetilde{d}$ is varied from 0.075 to 0.2. For all simulations, the most advanced fluid-fluid interface position along the fibers axis and most rearward one are tracked. They will be referred to as a and b respectively, using the notations introduced in section 3. At both positions, the pressure within the wetting fluid is extracted.

Since the values are extracted in the vicinity of the fluid-fluid interface, where the pressure is discontinuous, a specific procedure must be used to compute the value in the wetting fluid and at the interface. In this work the computation was achieved through a first order extrapolation of the pressure values in the wetting fluid and along the fiber axis direction. This procedure induces oscillations, especially when the pressure discontinuity is large (large La, small κ). Furthermore, local curvature errors can introduce additional oscillations in the overall pressure since it is computed using the Poisson equation resolution.

Their values $\widetilde{P}_a$ and $\widetilde{P}_b$ are plotted on figure 6a with the dimensionless time. In each simulation the pressure $\widetilde{P}_a$, $\widetilde{P}_b$, reach an asymptotic value before $\widetilde{t} \sim 100$. Asymptotic values are estimated by averaging pressures after $\widetilde{t} = 200$ and to the end of each simulation. Results are reported on figure 6b with the theoretical predictions presented in section 3. On the figure, the asymptotic pressures are in good agreement with Princen's model regardless of the spacing parameter. As a consequence, the pressure difference which drives the growth of capillary bridges is null when $\widetilde{d} \geq 0.15$ and negative otherwise. The dimensionless positions $\widetilde{X}_a$ and $\widetilde{X}_b$ along the axis of the fibers are tracked where pressures $\widetilde{P}_a$ and $\widetilde{P}_b$ were extracted. Results are presented on figure 6c. Due to the boundary conditions, the volume of each fluid within the computational domain is conserved. Therefore, the growth of capillary bridges gives rise to a backward motion of the wetting fluid in the middle of the unit cell (see figure 5b). Values of $\widetilde{X}_a$ and $\widetilde{X}_b$ reach asymptotic values when $\widetilde{d} \geq 0.15$ and do not overwise. On figure 6d the length $\Delta\widetilde{X} = \widetilde{X}_b - \widetilde{X}_a$ of the capillary bridges are reported with equation (16) predictions. According to the results, the long-time evolution of $\widetilde{X}$ stands within the predicted bounds. This regime is encountered after $\widetilde{t} \sim 100$, 500

depending on $\widetilde{d}$. Finally, within our dimensionless framework, the derivative of $\widetilde{X}$ with respect to $\widetilde{t}$ gives the capillary number Ca and $We = LaCa^2$. At $\widetilde{t} \sim 100$ the capillary and Weber numbers are $Ca \sim 3 \times 10^{-3}$, $We \sim 9 \times 10^{-2}$ and $\widetilde{X} \sim 2$. Then, Ca and We decrease with time. Therefore, the system is slender, the fluid-fluid interface is shaped by capillarity and the contact angle is constant such that the system meets the requirements of Princen's model. As discussed in section 3.2, these conditions explain the relevance of Princen's model in dynamics.

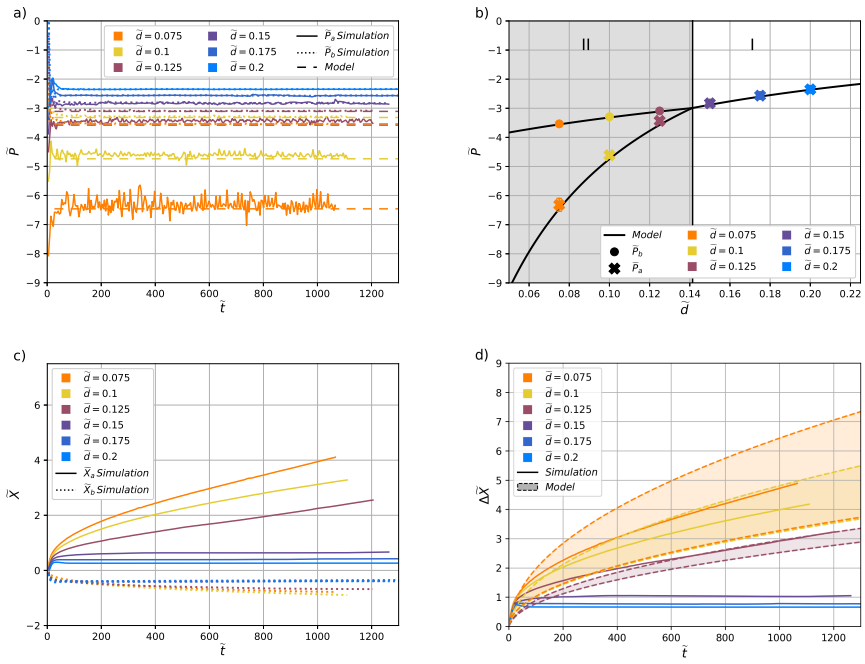

Figure 6: (a) Pressure $\widetilde{P}_a$ and $\widetilde{P}_b$ as functions of $\widetilde{t}$. (b) Princen's pressure predictions for a square lattice as a function of the spacing $\widetilde{d}$ with the computed pressures. In the domains (I) and (II) Princen's model predicts the non-existence and existence of capillary bridges respectively. (c) Positions of meniscus $\widetilde{X}$. (d) Capillary bridges lengths $\Delta\widetilde{X}$ as functions of $\widetilde{t}$. "Model" refers to the solution of equation (16), each simulation and the corresponding prediction are plotted with the same color

4.3. Influence of La

The Laplace number is varied from 1 to 10^5 with $\widetilde{d} = 0.1$. In figure 7a, $\widetilde{P}_a$ and $\widetilde{P}_b$ are plotted for all values of La. Their values converge and oscillate around Princen's prediction regardless of La. The length of capillary bridges $\Delta\widetilde{X}$ is displayed on figure 7b with the predictions of equation (16). For values of La ranging from 1 to 10^4, the curves overlap and are almost indistinguishable on the figure. For higher values, the effect of La on $\Delta\widetilde{X}$ is discernible in both the simulations and equation (16) predictions. The long-time evolution of $\Delta\widetilde{X}$ falls between the predicted bounds for all values of La but the simplistic model overstates widely its influence. However, according to the model, the transition time from an inertia dominated to a viscous dominated flow is a function of $\widetilde{\tau} = La\widetilde{K}$. As $\widetilde{K} \sim 3 \times 10^{-3}$ and the time required to reach the long-time evolution is $\widetilde{t} \sim 300$, the influence of La becomes sensible when $\widetilde{\tau} \sim 300$. This implies that inertia is negligeable as long as La is small ahead of 10^5. Although the model is not in good agreement with the reported results for $La = 10^5$, this value corresponds qualitatively to the transition from La-independent to La-dependent results. Furthermore, this transition value comes in contrast with the value of $\widetilde{\tau} = La/8$ in a circular capillary. In this case the permeability, $\widetilde{K}$, is about 40 times greater than in a capillary bridge due to the confinement of the wetting fluid between two solids close to each other and due to the chosen characteristic length. As a matter of illustration, the simulations presented in section 2.4 with $La = 50$ have a coefficient $\widetilde{\tau} = 6$; this value corresponds roughly to the one for the growth of capillary bridges between parallel fibers with $La = 1000$, $\widetilde{\tau} = 3$. Finally, the pressure differences are of comparable amplitude in both cases. As a consequence, the growth of a capillary bridge between two fibers of radius R is slower and less sensitive to inertia than the imbibition of a circular capillary of same radius. This second remark explains the low capillary and Weber numbers pointed out in the previous section.

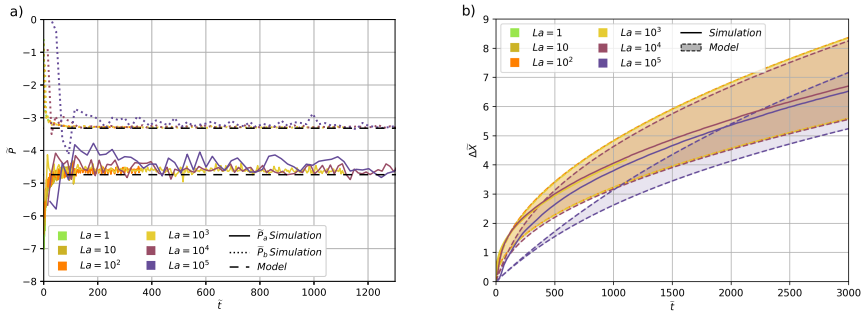

Figure 7: (a) Pressure $\widetilde{P}_a$ and $\widetilde{P}_b$ and (b) capillary bridges lengths $\Delta\widetilde{X}$ as functions of $\widetilde{t}$.

4.4. Influence of M_μ and M_ρ

To this point, the influence of the non-wetting fluid has not been considered. Indeed, the model of Bosanquet does not take into account the dissipation in or the momentum transferred to the second fluid. However, as its viscosity and density increase, its influence on the growth of capillary bridges should come into play. In this section, the density ratio M_ρ and the viscosity ratio M_μ are independently increased from 0.001 to 0.0316. The temporal evolution of pressures and the growth of capillary bridges are presented on figures 8a-d. According to the figures, the influence of M_ρ and M_μ on the pressures $\widetilde{P}_a$ and $\widetilde{P}_b$ are minute. Their influence on the lengths $\widetilde{X}_a$, $\widetilde{X}_b$ and thus on the capillary bridge length $\Delta\widetilde{X}$ are limited in the investigated range of values. However, comparing the sensitivity of lengths (figures 8b and 8d) M_μ has a stronger influence than M_ρ. For the set of parameters used, the confinement of liquid bridges makes the flow controlled by viscosity rather than inertia at the considered timescale. This explains the sensitivity difference observed. Finally, these overall weak influences of the second fluid on the flow show that neglecting the gas in a liquid-gas problem is relevant.

5. Fluid-fluid interface broadening in a set of parallel fibers

In real media where fibers are oriented in similar directions, there is no remarkable nor periodic lattice. In order to test the validity of the observations

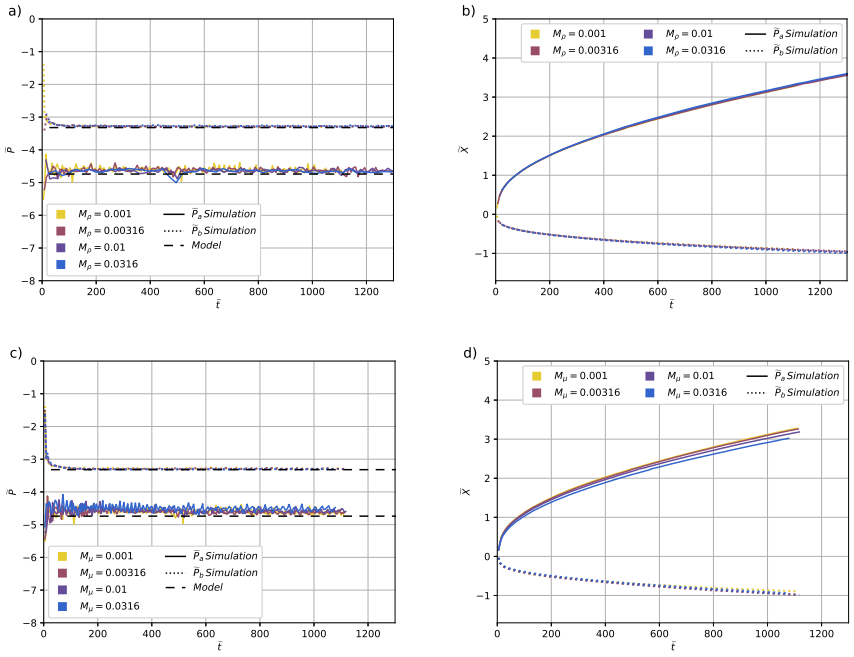

Figure 8: For different values of M_ρ, (a) pressures $\widetilde{P}_a$ and $\widetilde{P}_b$ as functions of $\widetilde{t}$, (b) capillary bridges lengths $\widetilde{X}$ as function of $\widetilde{t}$. For different values of M_μ, (c) pressures $\widetilde{P}_a$ and $\widetilde{P}_b$ as functions of $\widetilde{t}$, (d) capillary bridges lengths $\widetilde{X}$ as function of $\widetilde{t}$.

mentioned above, a more realistic case has been considered, the broadening of a fluid-fluid interface in a bunch of parallel fibers irregularly spaced from one another. In a domain of $8.8 \times 8.8 \times 5.5$, 12 fibers of radius $\widetilde{R} = 1$ have been set. Thus, the fiber volume ratio is $V_f = 0.49$, a value which may be encountered, for example, in composite materials applications (Abdalla et al., 2008; El Messiry, 2013). Their positions were picked from an isothermal molecular dynamics simulation of 12 particles in a 8.8×8.8 domain with periodic boundary conditions. Their initial positions and momentum were randomly picked and the simulation was stopped after a 10^4 iterations such that the distance traveled by each particle was greater than the domain size. Fibers sections are represented on figure 9. In the CFD domain, a flat fluid-fluid interface is initialized in a plane perpendicular to the axis of the fibers such that each fluid fills the same volume. A wall boundary condition is applied at the bottom and a zero-pressure boundary condition at the top. Periodic boundary conditions are applied to the other four boundaries. The domain is composed of $256 \times 256 \times 160$ mesh nodes. The physical parameters are set at the same values than the reference case studied in the previous section: the contact angle is $\theta_e = 10°$, the Laplace number to $La = 1000$ and $M_\rho = M_\mu = 10^{-3}$. On figure 9a the temporal evolution of the interface is shown. The interface is higher between close pairs of fibers. In order to simplify the discussion, on figure 9b the dimensionless height of the fluid-fluid interface is shown at the final time $\widetilde{t_f} = 175$, defined as the time at which the first capillary bridge reaches the upper boundary, and the fibers are numbered from 1 to 12. Capillary bridges exist between the pairs of fibers: $(9, 10)$, $(7, 9)$, $(5, 3)$, $(7, 10)$, $(8, 12)$, $(11, 12)$, $(5, 8)$, $(10, 12)$, $(4, 5)$ and the interface is slightly curved near the pairs: $(5, 7)$, $(2, 11)$, $(6, 9)$, $(1, 12)$, $(4, 6)$. No bridges are formed since the distances between these pairs are too large (see figure 10). For each fiber pair, the pressure near the fluid-fluid interface in the wetting fluid and between both fibers has been extracted and is reported on figure 10a. On the figure, most pressures converge quickly (at $\widetilde{t} \sim 10$) to values close to the theoretical prediction.

These predictions have been obtained through a modified version of Princen's

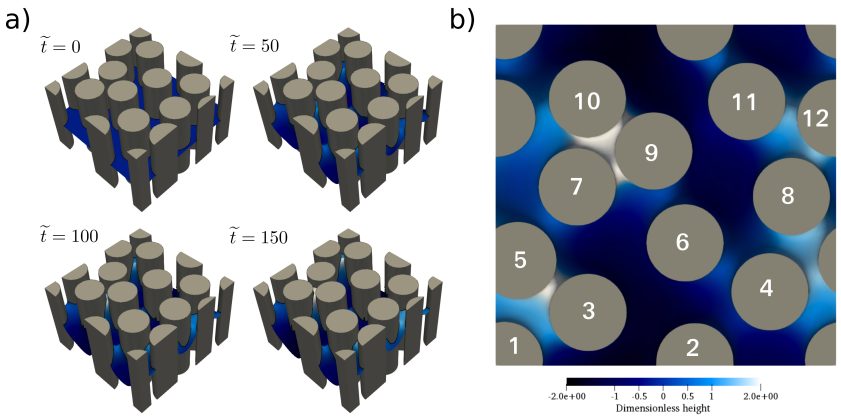

Figure 9: (a) Temporal evolution of the interface and (b) dimensionless height of the fluid-fluid interface in a set of random parallel set of fibers at time $\tilde{t} = 175$. See the Electronic Annex in the online version of this article for the corresponding video.

model presented in section 3.1 assuming that capillary bridges are formed only between pairs of fibers and that only a small fraction of the area of the fibers is in contact with capillary bridges. Under these two hypotheses, the pressure between pairs of fibers described by equation 11 and the pressure at the bottom of the domain writes

$$\widetilde{P}_I = -\frac{2N\pi\cos(\theta_e)}{(L^2 - N\pi)}, \tag{17}$$

with N the number of fibers and L the domain width. These values are plotted on figure 10b with the extract ones, averaged from $\widetilde{t} = 25$ to $\widetilde{t} = 175$ as functions of the spacing parameter $\widetilde{d}$. Overall, the results are in good agreement with the theoretical predictions despite the simplicity of the model. However, for the fiber pair $(7, 10)$, the pressure is widely underestimated by the fiber pair model. As it may be seen on figure 9b, the fibers $(7, 9, 10)$ are packed into a triangle. Therefore, the fiber pair model is not adapted to this case. Furthermore, between pairs $(11, 12)$ and $(8, 5)$ the pressure is lower in the simulation and does not seem to depend on the spacing parameter. This observation has been attributed to the growing influence of neighboring fibers as the spacing

increase. The model for three fibers forming an equilateral triangle, described in (Princen, 1969b), is reported on the figure. It shows that most values stands between both models. The dimensionless heights $\widetilde{X}$ of capillary bridges are reported in figure 10c. These values are defined as null when $\widetilde{t} = 0$. As the volume of capillary bridges are small compared to the overall wetting fluid volume, the receding motion of the interface is minute. Thus, the length of one bridge can the roughly assessed by $\widetilde{X}$. On the figure, the growth of capillary bridges $(9, 10)$ and $(7, 9)$ are the fastest followed by the capillary bridges $(7, 10)$ and $(3, 5)$ and then by the others. This order is correlated to the distance between fibers and is consistent with the results presented in section 4. It confirms that the growth of capillary bridges is improved by the proximity of fibers. Furthermore, the growths between fiber pairs $(9, 10)$, $(3, 5)$, $(8, 12)$ and $(10, 12)$ are also compared to Bosanquet's model prediction on the figure. Once again, the results are in qualitative agreement with the theory despite the simplicity of the model.

6. Conclusion

The in-house code ARCHER has been extended to handle a static contact angle in a two-phase flow with an immersed solid. The numerical method implemented describes properly the spreading of a droplet on a flat substrate and the spontaneous imbibition of a circular capillary. This method has been applied to model the growth of capillary bridges in sets of parallel fibers. The model of (Princen, 1969b) predicts the existence of pressure differences in remarkable lattices which correspond to capillary bridges at the hydrostatic equilibrium. In the literature, multiple authors generalized the analysis to various geometries (Protiere et al., 2013; Soleimani et al., 2015; Boulogne et al., 2015; Sauret et al., 2015) and showed that it is quite robust. In the present work, the relevance of this model in dynamics is questioned and the growth of capillary bridges is described and modeled. Finally, the sensitivity of these results with respect to the degree of order in the lattice is questioned. Based on the reported set of numerical simulations, the main conclusions reported here are that:

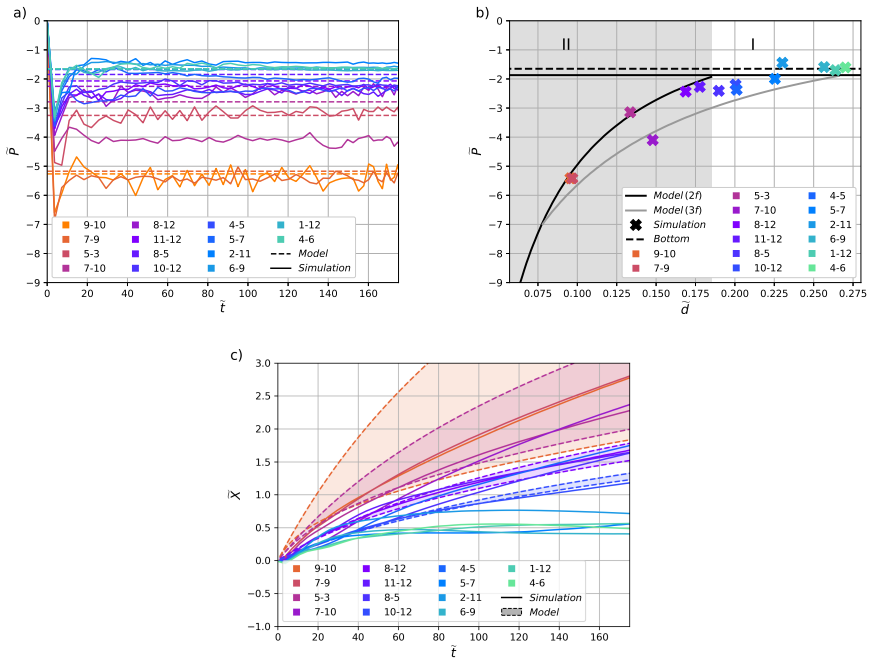

Figure 10: (a) Dimensionless pressure at the tip of capillary bridges as functions of $\widetilde{t}$. "Model" refers the prediction described in section 3.1 (b) Average pressures as a function of the spacing . "Model (2f)" refers to the pressure predicted at the tip of capillary bridges (described in section 3.1) and "Model (3f)" to the prediction in a triangle of fibers (described in (Princen, 1969b)). (c) Heights of capillary bridges as functions of $\widetilde{t}$. "Model" refers to the solutions of equation (16)

- Princen's model provides accurate predictions in dynamics. The robustness of Princen's model can be understood as a consequence of the high degree of confinement that exists between the fibers.

- The non-wetting phase plays a negligible role in a liquid-gas system. As a consequence, the growth of capillary bridges is in qualitative agreement with the predictions of Bosanquet's model. In comparison with the imbibition of a circular capillary, inertia has a negligible influence on the flow.

- In a disordered lattice of parallel fibers with a fiber volume ratio of 0.49, the pressures and growths of capillary bridges between pairs of fibers are in an overall qualitative agreement with Princen's and Bosanquet's model respectively. According to this conclusion, in a slow drainage or imbibition, the fluid-fluid interface width W in a yarn is expected to scale as $W \propto \sqrt{t}$. Nonetheless, this point relies on a single computation and should be further confirmed.

Acknowledgements

This work was granted access to the HPC resources of IDRIS, TGCC and CINES under the allocation A0052B10101 made by GENCI (Grand Equipement National de Calcul Intensif). The supercomputer center CRIANN (Centre Régional Informatique et d'Applications Numériques de Normandie) under the scientific project No. 201 704 is also gratefully acknowledged.

Appendix A. Appendix

In a capillary bridge between a pair of fibers, the area occupied by the wetting fluid is represented on figure A.11. Only a quarter of the system is represented and the curvature of the fluid-fluid interface is not considered. Half the spacing

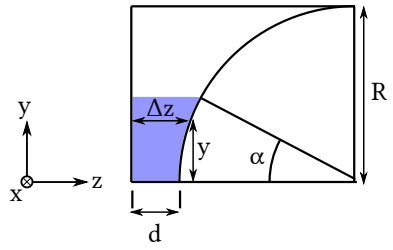

Figure A.11: Sketch of a quarter of the area considered in the permeability computation.

$\Delta\widetilde{z}$ between the fibers is:

$$\Delta\widetilde{z} = \widetilde{d} + \left(1 - \sqrt{1-\widetilde{y}^2}\right). \tag{A.1}$$

According to Princen's computation, the angle α is small when capillary bridges exist. Therefore, $\widetilde{y}$ is small as well and this equation may be approximated at order 3 in $\widetilde{y}$ to:

$$\Delta\widetilde{z} \approx \widetilde{d} + \frac{\widetilde{y}^2}{2}. \tag{A.2}$$

The filled area is:

$$\widetilde{S} = 4\int_{\widetilde{y}=0}^{\widetilde{y}=\alpha}\int_{\widetilde{z}=0}^{\widetilde{z}=\widetilde{d}+\frac{\widetilde{y}^2}{2}} d\widetilde{z}d\widetilde{y} = 4\widetilde{d}\alpha + \frac{2}{3}\alpha^3. \tag{A.3}$$

As a consequence of the slow spatial variation of $\Delta\widetilde{z}$ with $\widetilde{y}$, a plane Hagen-Poiseuille flow is assumed to take place. Therefore, the velocity along the fiber axis is given by

$$\widetilde{v}(\widetilde{z},\widetilde{y}) = -\frac{\partial\widetilde{P}}{\partial\widetilde{x}}\frac{1}{2\mu}\left(\left(\widetilde{d}+\frac{\widetilde{y}^2}{2}\right)^2 - \widetilde{z}^2\right), \tag{A.4}$$

and overall flow rate by

$$\widetilde{Q} = 4\int_{\widetilde{y}=0}^{\widetilde{y}=\alpha}\int_{\widetilde{z}=0}^{\widetilde{z}=\widetilde{d}+\frac{\widetilde{y}^2}{2}} \widetilde{v}(\widetilde{z},\widetilde{y})d\widetilde{z}d\widetilde{y} = \left(-\frac{1}{\mu}\frac{\partial\widetilde{P}}{\partial\widetilde{x}}\right)\frac{2}{3}\left(\left(\widetilde{d}+\frac{\alpha^2}{2}\right)^4 - \widetilde{d}^4\right). \tag{A.5}$$

Finally, the corresponding permeability is

$$\widetilde{K} = \frac{\left(\widetilde{d} + \frac{\alpha^2}{2}\right)^4 - \widetilde{d}^4}{6\widetilde{d}\alpha + \alpha^3} \tag{A.6}$$

and it can be computed at the bottom or at the tip of each capillary bridge using the local value of α.

References

References

Abdalla, F., Megat, M., Sapuan, M., Sahari, B., 2008. Determination of volume fraction values of filament wound glass and carbon fiber reinforced composites. ARPN Journal of Engineering and Applied Sciences 3, 7–11.

Aboukhedr, M., Georgoulas, A., Marengo, M., Gavaises, M., Vogiatzaki, K., 2018. Simulation of micro-flow dynamics at low capillary numbers using adaptive interface compression. Computers & Fluids , –.

Akai, T., Bijeljic, B., Blunt, M.J., 2018. Wetting boundary condition for the color-gradient lattice boltzmann method: Validation with analytical and experimental data. Advances in water resources 116, 56–66.

Arienti, M., Sussman, M., 2014. An embedded level set method for sharp-interface multiphase simulations of diesel injectors. International Journal of Multiphase Flow 59, 1 – 14.

Asuri Mukundan, A., Ménard, T., Berlemont, A., Brändle de Motta, J.C., Eggels, R., 2019. Validation and analysis of 3d DNS of planar pre-filming airblast atomization simulations, in: In Proceedings of ILASS Americas, 30th Annual Conference on Liquid Atomization and Spray Systems. May 12th-15th, Tempe, Arizona, USA.

Biance, A.L., Clanet, C., Quéré, D., 2004. First steps in the spreading of a liquid droplet. Physical Review E 69, 016301.

Bico, J., Roman, B., Moulin, L., Boudaoud, A., 2004. Elastocapillary coalescence in wet hair. Nature 432, 690.

Bird, J., Mandre, S., Stone, H., 2008. Short-time dynamics of partial wetting. Physical review letters 100, 234501.

Bosanquet, C., 1923. On the flow of liquids into capillary tubes. The London, Edinburgh, and Dublin Philosophical Magazine and Journal of Science 45, 525–531.

Boulogne, F., Sauret, A., Soh, B., Dressaire, E., Stone, H., 2015. Mechanical tuning of the evaporation rate of liquid on crossed fibers. Langmuir 31, 3094–3100.

Chandra, D., Yang, S., 2009. Capillary-force-induced clustering of micropillar arrays: is it caused by isolated capillary bridges or by the lateral capillary meniscus interaction force? Langmuir 25, 10430–10434.

Chebbi, R., 2007. Dynamics of liquid penetration into capillary tubes. Journal of Colloid and Interface Science 315, 255–260.

Chen, N., Wu, J., Jiang, H., Dong, L., 2012. CFD simulation of droplet formation in a wide-type microfluidic T-junction. Journal of Dispersion Science and Technology 33, 1635–1641.

Concus, P., Finn, R., 1969. On the behavior of a capillary surface in a wedge. Proceedings of the National Academy of Sciences of the United States of America 63, 292.

Dickerson, A., Mills, Z., Hu, D., 2012. Wet mammals shake at tuned frequencies to dry. Journal of the Royal Society Interface 9, 3208–3218.

Digilov, R., 2008. Capillary rise of a non-newtonian power law liquid: Impact of the fluid rheology and dynamic contact angle. Langmuir 24, 13663–13667.

Dubé, M., Daneault, C., Vuorinen, V., Alava, M., Rost, M., 2007. Front roughening in three-dimensional imbibition. The European Physical Journal B 56, 15–26.

Duprat, C., Protiere, S., Beebe, A., Stone, H., 2012. Wetting of flexible fibre arrays. Nature 482, 510.

El Messiry, M., 2013. Theoretical analysis of natural fiber volume fraction of reinforced composites. Alexandria Engineering Journal 52, 301–306.

Figliuzzi, B., Buie, C.R., 2013. Rise in optimized capillary channels. Journal of Fluid Mechanics 731, 142–161.

Fries, N., Dreyer, M., 2008. The transition from inertial to viscous flow in capillary rise. Journal of colloid and interface science 327, 125–128.

de Gennes, P., 1985. Wetting: statics and dynamics. Rev. Mod. Phys. 57, 827–863.

Horváth, V., Stanley, H., 1995. Temporal scaling of interfaces propagating in porous media. Physical Review E 52, 5166.

Hultmark, M., Aristoff, J., Stone, H., 2011. The influence of the gas phase on liquid imbibition in capillary tubes. Journal of Fluid Mechanics 678, 600–606.

Legendre, D., Maglio, M., 2013. Numerical simulation of spreading drops. Colloids and Surfaces A: Physicochemical and Engineering Aspects 432, 29–37.

Lepilliez, M., Popescu, E.R., Gibou, F., Tanguy, S., 2016. On two-phase flow solvers in irregular domains with contact line. Journal of Computational Physics 321, 1217–1251.

Malgarinos, I., Nikolopoulos, N., Marengo, M., Antonini, C., Gavaises, M., 2014. Vof simulations of the contact angle dynamics during the drop spreading: Standard models and a new wetting force model. Advances in colloid and interface science 212, 1–20.

Ménard, T., Tanguy, S., Berlemont, A., 2007. Coupling level set/VOF/ghost fluid methods: Validation and application to 3d simulation of the primary break-up of a liquid jet. International Journal of Multiphase Flow 33, 510–524.

Ng, Y., Min, C., Gibou, F., 2009. An efficient fluid–solid coupling algorithm for single-phase flows. Journal of Computational Physics 228, 8807–8829.

Patnaik, A., Rengasamy, R., Kothari, V., Ghosh, A., 2006. Wetting and wicking in fibrous materials. Textile Progress 38, 1–105.

Pokroy, B., Kang, S., Mahadevan, L., Aizenberg, J., 2009. Self-organization of a mesoscale bristle into ordered, hierarchical helical assemblies. Science 323, 237–240.

Ponomarenko, A., Quéré, D., Clanet, C., 2011. A universal law for capillary rise in corners. Journal of Fluid Mechanics 666, 146–154.

Princen, H., 1969a. Capillary phenomena in assemblies of parallel cylinders: I. Capillary rise between two cylinders. Journal of Colloid and Interface Science 30, 69–75.

Princen, H., 1969b. Capillary phenomena in assemblies of parallel cylinders: II. Capillary rise in systems with more than two cylinders. Journal of Colloid and Interface Science 30, 359–371.

Protiere, S., Duprat, C., Stone, H., 2013. Wetting on two parallel fibers: drop to column transitions. Soft Matter 9, 271–276.

Pucci, M., Liotier, P.J., Drapier, S., 2017. Wicking tests for unidirectional fabrics: Measurements of capillary parameters to evaluate capillary pressure in liquid composite molding processes. JoVE (Journal of Visualized Experiments) , e55059.

Quéré, D., 1997. Inertial capillarity. Europhysics Letters (EPL) 39, 533–538.

Reyssat, M., Courbin, L., Reyssat, E., Stone, H., 2008. Imbibition in geometries with axial variations. Journal of Fluid Mechanics 615, 335.

Sadeghi, R., Safdari Shadloo, M., Hopp-Hirschler, M., Hadjadj, A., Nieken, U., 2018. Three-dimensional lattice boltzmann simulations of high density ratio two-phase flows in porous media. Computers & Mathematics with Applications .

Sadjadi, Z., Rieger, H., 2013. Scaling theory for spontaneous imbibition in random networks of elongated pores. Physical review letters 110, 144502.

Sauret, A., Boulogne, F., Cébron, D., Dressaire, E., Stone, H., 2015. Wetting morphologies on an array of fibers of different radii. Soft Matter 11, 4034–4040.

Soleimani, M., Hill, R., van de Ven, T., 2015. Capillary force between flexible filaments. Langmuir 31, 8328–8334.

Sussman, M., Smith, K., Hussaini, M., Ohta, M., Zhi-Wei, R., 2007. A sharp interface method for incompressible two-phase flows. Journal of Computational Physics 221, 469–505.

Tang, L.H., Tang, Y., 1994. Capillary rise in tubes with sharp grooves. Journal de Physique II 4, 881–890.

Tanner, L., 1979. The spreading of silicone oil drops on horizontal surfaces. Journal of Physics D: Applied Physics 12, 1473.

Testoni, G., Kim, S., Pisupati, A., Park, C., 2018. Modeling of the capillary wicking of flax fibers by considering the effects of fiber swelling and liquid absorption. Journal of colloid and interface science 525, 166–176.

Vaudor, G., Ménard, T., Aniszewski, W., Doring, M., Berlemont, A., 2017. A consistent mass and momentum flux computation method for two phase flows. Application to atomization process. Computers & Fluids 152, 204–216.

Vu, T.T., 2017. Atomisation process of turbulent liquid sheets : Experimental analyses and numerical developments. phdthesis. Normandy University.

Walls, P., Dequidt, G., Bird, J., 2016. Capillary displacement of viscous liquids. Langmuir 32, 3186–3190.

Wang, P., Bian, R., Meng, Q., Liu, H., Jiang, L., 2017. Bioinspired dynamic wetting on multiple fibers. Advanced Materials 29, 1703042.

Wang, S., Desjardins, O., 2018a. 3d numerical study of large-scale two-phase flows with contact lines and application to drop detachment from a horizontal fiber. International Journal of Multiphase Flow 101, 35–46.

Wang, S., Desjardins, O., 2018b. Numerical study of the critical drop size on a thin horizontal fiber: Effect of fiber shape and contact angle. Chemical Engineering Science 187, 127–133.

Washburn, E., 1921. The dynamics of capillary flow. Physical review 17, 273.

Wilkinson, D., 1984. Percolation model of immiscible displacement in the presence of buoyancy forces. Physical Review A 30, 520.

Winkels, K.G., Weijs, J.H., Eddi, A., Snoeijer, J.H., 2012. Initial spreading of low-viscosity drops on partially wetting surfaces. Physical Review E 85, 055301.

Xu, S., Ren, W., 2016. Reinitialization of the Level-Set Function in 3d Simulation of Moving Contact Lines. Communications in Computational Physics 20, 1163–1182.

Yokoi, K., Vadillo, D., Hinch, J., Hutchings, I., 2009. Numerical studies of the influence of the dynamic contact angle on a droplet impacting on a dry surface. Physics of Fluids 21, 072102.